UC Berkeley

Title

Megaphylogeny resolves global patterns of mushroom evolution

Permalink

Journal

ISSN

Authors

Varga, Torda
Krizsán, Krisztina
Földi, Csenge
et al.

Publication Date

DOI

Peer reviewed

Megaphylogeny resolves global patterns of mushroom evolution

A full list of authors and affiliations appears at the end of the article.

Abstract

Mushroom-forming fungi (Agaricomycetes) have the greatest morphological diversity and complexity of any group of fungi. They have radiated into most niches and fulfill diverse roles in the ecosystem, including wood decomposers, pathogens or mycorrhizal mutualists. Despite the importance of mushroom-forming fungi, large-scale patterns of their evolutionary history are poorly known, in part due to the lack of a comprehensive and dated molecular phylogeny. Here, using multigene and genome-based data, we assemble a 5,284-species phylogenetic tree and infer ages and broad patterns of speciation/extinction and morphological innovation in mushroom-forming fungi. Agaricomycetes started a rapid class-wide radiation in the Jurassic, coinciding with the spread of (sub)tropical coniferous forests and a warming climate. A possible mass extinction, several clade-specific adaptive radiations, and morphological diversification of fruiting bodies followed during the Cretaceous and the Paleogene, convergently giving rise to the classic toadstool morphology, with a cap, stalk, and gills (pileate-stipitate morphology). This morphology is associated with increased rates of lineage diversification, suggesting it represents a key innovation in the evolution of mushroom-forming fungi. The increase in mushroom diversity started during the Mesozoic-Cenozoic radiation event, an era of humid climate when terrestrial communities dominated by gymnosperms and reptiles were also expanding.

*Correspondence to: lnagy@fungenomelab.com.
&Current address: Institute of Ecology and Earth Sciences, University of Tartu, Tartu, Estonia
&&Current address: MTA-SZTE 'Lendulet' Fungal Pathogenicity Mechanisms Research Group, Kozep fasor 52, 6726 Szeged, Hungary
#Current address: Section for Genetics and Evolutionary Biology (EVOGENE), University of Oslo, Blindernveien 31, 0316 Oslo, Norway

Explosive diversification events, with intermittent periods of relatively little change, have generated uneven patterns of species richness across the tree of life. Although rapid radiations have been inferred in many clades1–5, few examples exist for fungi, in part because of their limited fossil record, and the lack of comprehensive phylogenies. Advances in modeling the evolutionary process now allow such inferences to be made from phylogenetic trees. Studies of diversification of mushroom-forming fungi have focused on individual clades6–9, yielding hypotheses on ecological opportunities6, the evolution of mutualistic lifestyle7,10 and fruiting body morphologies6,11 as drivers of adaptive evolution in fungi. However, these inferences, based on specific clades, remained untested across larger phylogenetic scales. Fruiting bodies provide support and protection for developing spores, which probably represents a driving force for increasingly more efficient morphologies12. Ancestral fruiting bodies of the Agaricomycotina were probably crust-like, 'resupinate' forms13,14, which then evolved into increasingly more complex forms, including derived 'pileate-stipitate' types, which are differentiated into a cap, stipe and hymenophore (spore-bearing surface). Pileate-stipitate forms have arisen repeatedly from simpler morphologies (e.g. resupinate or coral-like) during evolution12,13,15 and dominate extant agaricomycete diversity (>21,000 described species16), but how this diversity arose, what explains the dominance of pileate-stipitate species in the class and whether fruiting body morphology impacts diversification rates (e.g. as a key innovation) are not known.

Results and Discussion

We investigated broad patterns of diversification in Agaricomycetes using a phylogenetic comparative approach and generated the most comprehensive phylogeny of the group to date, comprising 5,284 species (Fig. 1). Our dataset represents ca. 26% of described Agaricomycetes, the highest sampling density reported for any fungal group to date. Our inferences of phylogenetic trees combine a robust genome-based backbone phylogeny of 104 species (650 genes, 141,951 amino acid characters, Supplementary Fig. 1-3, Supplementary Table 1, Supplementary Note 1,2) with sequence data from up to three nuclear loci for 5,284 taxa (LSU rRNA, rpb2, ef-1a, 5,737 characters). New sequence data were generated for 1,222 species (Supplementary Note 2, Supplementary Data 1), including 9 new genomes of phylogenetically key taxa (Supplementary Note 3). The phylogenetic tree topology is largely congruent with previously published clade-specific phylogenies and resolves 21 orders of Agaricomycetes plus Dacrymycetes and Tremellomycetes as outgroups. Most of the nodes received strong bootstrap support, but we also identified nodes that require more scrutiny and probably denser taxon sampling to be resolved with certainty (for a detailed genome-based overview of agaricomycete phylogeny see Supplementary Note 1). We inferred ten time-calibrated phylogenies for the 5,284 taxa dataset using a 2-stage Bayesian approach and all taxonomically informative, non-conflicting fossil calibration points available in the Agaricomycetes (eight fossils, determined by a fossil cross-validation procedure, see Supplementary Fig. 4, Supplementary Table 2, Supplementary Note 4). Inferred node heights of the order-level clades range from 183 to 71 Myr, which places the origin of most order-level clades in the Jurassic, with the Cantharellales (mean age: 184 Myr,144-261 Myr across ten chronograms), Agaricales (mean: 173 Myr, 160-182 Myr), Hymenochaetales (mean: 167 Myr, 130-180 Myr) and Boletales (mean: 142 Myr, 133-153

Myr) being the oldest. The Agaricomycetidae, the group uniting the Agaricales and Boletales was estimated at ~185 Myr (174-192, Fig. 1, Supplementary Note 4). Because these molecular clock estimates are older than previous phylogenomics-based figures[17–19], we performed sensitivity analyses to address the underlying causes, which suggest that the differences are attributable to the higher taxon sampling density in both our genome-based and 5,284-species tree and not to differences in software or choice of priors in fossil-based molecular clock calibrations. Various taxon and fossil sampling schemes, tree (5,284-taxon versus the genome-based phylogeny) and software choice had little impact on inferred ages (Supplementary Data 2, Supplementary Note 4), providing a robust set of age estimates for Agaricomycetes.

We analyzed global rates of speciation and extinction in a macroevolutionary framework using BAMM[20]. We accounted for incomplete and unequal sampling by using clade-specific sampling fractions and by ensuring that each genus is sampled in proportion to the number of its described species. Analyses of diversification rates in ten time-calibrated phylogenies provided evidence for rate variation through time and across lineages. Diversification rates increased abruptly at ~180 Myr ago in the early Jurassic (Fig. 2), coinciding with the breakup of Pangea, the onset of a warm, humid climate and the spread of (sub)tropical gymnosperm forests. Consistent with this, ancestral state reconstructions suggest that the last common ancestors of most orders were likely associated with gymnosperms as hosts (Fig. 1, Fig. 3/a, Supplementary Data 3, Supplementary Note 5), followed by multiple shifts to and diversification in association with angiosperms as hosts during the Cretaceous, similar to patterns observed in a radiation of herbivorous beetles[21]. This agrees with observations of fungus-plant co-evolution at smaller scales[10,22], frequent host switches during fungal evolution[23] and might reflect the dependence of fungi on plants as nutrient sources or mutualistic partners.

Acceleration of speciation is observed across all larger orders (Supplementary Data 4), suggestive of an external underlying cause, such as climate change or nutrient availability, instead of clade-specific events. We find that the rise in speciation rates in the Jurassic is coupled with a slightly delayed increase in extinction rates ~150 mya (Fig. 2). Although estimating extinction rates from phylogenies is notoriously difficult[24–26], this signal is also detected in an independent analysis using an episodic speciation/extinction model[27] under a variety of conditions (Supplementary Note 6, Supplementary Fig. 6, Supplementary Table 3,4). Together, these data suggest that fungi experienced severe extinction in a period that falls close to a mass extinction event at the Jurassic/Cretaceous boundary[28], an era with a fluctuating edaphic conditions, differential extinction of several metazoan groups, and a relatively stable flora. On the other hand, we find no evidence for increased probability of extinction around the Cretaceous-Tertiary (K-T) boundary, a period of severe mass extinction in plant and animal lineages. It has been hypothesized that the massive deforestation after the bolide impact has buffered fungi through the period[29], which is supported by a peak in fungal spore and hyphae fossilization right after the cataclysm[30] and would explain the lack of mass extinction signal in our data.

The latitudinal diversity gradient (LDG) hypothesis posits that species richness increases from the poles towards the tropics. To test if this general prediction is valid for

Agaricomycetes, we analyzed latitude-dependent diversification rates across all 4,429 species for which sufficient geographic data could be obtained (see Methods). Agaricomycetes display their highest species diversity and net diversification rates in the temperate zone (Supplementary Fig. 7,8, Supplementary Table 5,6, Supplementary Note 7), which contrasts with the diversity gradient from the poles towards the tropics in animals and plants[31]. Although such a pattern could arise as a result of more concentrated efforts of recording fungi in the temperate zone, we find that the zone with highest speciation rate (between 20° and 40° in the temperate zone) does not coincide with the zone of the highest sampling density (30°–60°) in our data. This suggests that our inference of a temperate peak in diversification rates is largely independent from sampling density. A reversed latitudinal diversity gradient has already been implied for major fungal groups by several surveys of environmental sequences[32–34] and phylogenetic analyses[22,35], in particular for ectomycorrhizal fungi. Although such signals might also be sensitive to biased taxonomic efforts across ecoregions, these data suggest that Agaricomycetes might not conform to broad macroecological patterns that dominate in animal and plant lineages.

To obtain a more resolved picture on diversification histories, we analyzed rate variation across clades. We identified 85 significant shifts in diversification rate (defined as shifts present in 50% of trees with marginal odds ratio 5) that included clades of diverse ages spread out across the Agaricomycetes (Fig. 1, Supplementary Data 5, Supplementary Fig. 9,10, Supplementary Table 7,8, Supplementary Note 8). The largest of these comprises the Agaricomycetidae, consistent with results of rate through time and lineages through time analyses, which revealed an acceleration of net diversification rates in the Jurassic (Fig. 2). Order-level shifts to higher diversification rates were inferred in the last common ancestor of the Auriculariales, that of the Cantharellales, the Hymenochaetales (excluding the Repetobasidiaceae), the Russulales and the Agaricales (excluding the hygrophoroid and pleurotoid clades (sensu Matheny[15]) (Fig. 1). Most of the shifts (67%) were found in the Agaricales and predominantly in the Paleogene, consistent with a dynamic evolutionary history of the order but also with its largest share of diversity in the class. We found accelerated diversification in the genera *Coprinellus* and *Laccaria*, as reported previously[6,7], but also in *Cortinarius, Amanita* and *Lepiota*, among others (for the complete list of shifts see Supplementary Data 5). Some of these represent the most taxonomically diverse agaric genera, such as *Cortinarius* with >2,000[16] species described. Accelerated diversification in these groups is consistent with patterns seen in adaptive radiations[36,37]. Indeed, many clades show a diversification slowdown through time, a key sign of adaptive radiations[36] (Supplementary Data 6), suggesting that many of the detected shifts may feature rapid adaptive filling of available niches. Among the 85 detected shifts in diversification rates, there were several that denoted old clades with low diversity, in which the shift represents a diversification slowdown rather than acceleration. For example, the genus *Typhula*, comprising species with minute club-shaped fruiting bodies, is an ancient group (dated at ca. 76 myr) with a low diversity and an inferred diversification slowdown along its stem branch. Such parameters may indicate clades of relict lineages rooting deeply in Agaricales history but having only a few extant representatives. Taken together, these analyses provide a global view on bursts and slowdowns in the diversification history of mushroom-forming fungi and

should facilitate a better understanding of adaptive diversification events in fungi, of which only a single example has been explicitly demonstrated6.

We next asked how morphological innovations may have contributed to shape the extant diversity of Agaricomycetes. Because fruiting body complexity is an important adaptive trait13,14, we mapped the evolution of fruiting body morphologies on the phylogeny and examined its impact on diversification rates. We performed ancestral state reconstructions and summarized inferred ancestral states through time across ten chronograms (Fig. 3/b). In line with previous studies13,14, our reconstructions suggest ancestors with resupinate (crust-like) fruiting bodies for most early nodes along the backbone of the Agaricomycetes. The early dominance of resupinate morphologies was rapidly taken over by an array of more complex morphologies in the late Jurassic (~170-180 myr), of which the pileate-stipitate type appears most dominant. This pattern could have been driven by the radiation of Agaricomycetidae, which contains the majority of pileate-stipitate species and started to diversify around this period, although pileate-stipitate species evolved in 12 orders as well, including the Russulales, Cantharellales and Gloeophyllales, among others. In the meanwhile, resupinate lineages may have simply continued to diversify at their previous rate, but, because of the radiation of species with pileate-stipitate fruiting bodies their dominance was diminished at the scale of the entire class. Consistent with this view, gains of the pileate-stipitate morphology are estimated to be significantly more likely (7-50 times, logBayes-factor, logBF = 47) than their loss, indicating a trend towards pileate-stipitate morphologies, as reported earlier13. In fact, the pileate-stipitate morphology evolved convergently in at least 33 clades, suggesting it represents a stable attractor in the morphospace. Nevertheless, the probability of the loss of pileate-stipitate morphology is significantly larger than zero (logBF = 157.2), reflecting evolutionary transformations of pileate-stipitate fruiting bodies happening in many groups (Fig. 3/c, Supplementary Data 1,7). We tested the impact of fruiting body morphologies on diversification rate in a character-state dependent speciation and extinction framework38,39. Clades with pileate-stipitate fruiting bodies have a significantly higher speciation rate ($P<10^{-16}$, Likelihood Ratio Test, LRT) than clades with other morphologies (Fig. 3/d, Supplementary Data 7). This may be because the pileate-stipitate morphology provides support and protection for developing spores (e.g. from precipitation) and enhances their dispersal efficiency by raising sporogenous tissue above ground-level; these advantages may explain how pileate-stipitate fruiting bodies can promote diversification and suggest they represent a key innovation for mushroom-forming fungi.

Conclusions

This study represents a global analysis of the dynamic evolutionary history of mushroom-forming fungi. The diversity of Agaricomycetes might have been shaped by both class-wide diversification rate shifts and explosive clade-specific events. We identified a major class-wide radiation of Agaricomycetes in the Jurassic, which possibly followed a warming and humid climate in this period. The onset of this radiation coincided with the expansion of angiosperms and followed patterns of gymno- and later angiosperm expansion during the Mesozoic-Cenozoic radiation40. Our analyses provide evidence for several clade-specific adaptive radiations in the class, providing a possible explanation for why some genera

contain a single while others thousands of species. Our data display strong signal for a mass extinction event coinciding with increased extinction rates at the Jurassic/Cretaceous boundary, however, no such evidence was found in the Agaricomycetes for the much more influential K-T mass extinction event. The evolution of pileate-stipitate fruiting bodies, i.e., morphologies with cap and stipe might be a key driver of evolutionary radiations, suggesting that the convergent evolution of the classic mushroom morphology contributed to shaping extant diversity in the Agaricomycetes. We predict that further data on traits and ecological opportunities that generated the spectacular diversity of mushroom-forming fungi will help to elucidate the general principles of mushroom evolution and integrate this ecologically important group into the record of major biodiversification events.

Methods

1 Molecular biology methods

Genomic DNA was extracted from 0.1 - 10 mg of dried herbarium specimens using the DNeasy Plant Mini kit (Qiagen) or the Nucleospin Plant II mini kit (Macherey-Nagel) following the manufacturers' instructions. PCR amplification was performed as described previously[6,15] on the large subunit of (LSU) of the nuclear ribosomal RNA with the LR7 and LROR primers. Sequencing was performed commercially using the same primers as used for PCR. Sanger reads were assembled to a contig using the Pregap and Gap4 programs of the Staden package[43] and checked manually against the electropherograms.

2 Taxon sampling

We sampled herbarium specimens so that taxon sampling be proportional across clades and geographic regions. To that end, we initially obtained estimates of the known diversity for each of the genera from Species Fungorum[44] (www.speciesfungorum.org, accessed 8.24.2015), the Dictionary of the Fungi[16] and from Funga Nordica[45]. Taxonomic information from these sources was compiled for all genera of Agaricomycetes. Using this compilation, we calculated the number of target species that needed to be sampled for each genus to obtain a final dataset of ~5,000 species (~30% sampling of total diversity) in which sampling of species in each genus is proportional to their described diversity. Although the three sources differed in their completeness, geographic scope (Dictionary of the Fungi and Species Fungorum being global databases and Funga Nordica being taxonomically most stringent of the three) and taxonomic concept, it gave us general guidance on how to keep taxon sampling proportional across genera. While sampling species within genera, attempts have been made to obtain specimens from undersampled geographic regions, in particular Africa, Asia, Australasia and South America.

3 Sequence alignment

Multiple sequence alignment was carried out for the LSU, ef-1a and RPB2 loci separately using the Probabilistic Alignment Kit (PRANK release 140603)[46,47]. An iterative alignment refinement strategy as described in Tóth et al.[48] was employed: ML gene trees computed from preliminary alignments (using RAxML, see below) were used as guide trees for the next round of multiple alignment for PRANK. After three rounds of iterative refinement, the alignments were further corrected manually using a text editor. Manual

curation was restricted to correcting homologous regions erroneously juxtaposed by PRANK. Alignments of individual sequences were concatenated into a superalignment. The concatenated alignment is available at Dryad (Accession Number XXXX to be provided upon publication), GenBank accession numbers for all sequences used are shown in Supplementary Data 1.

4 Genome and transcriptome sequencing and assembly

4.1 Sequencing—The genomes of *Coprinopsis marcescibilis*, *Crucibulum leave*, *Dendrothele bispora*, *Heliocybe sulcata*, *Peniophora* sp., *Pluteus cervinus*, *Polyporus arcularius* and *Pterula gracilis* were sequenced using a combination of fragment and long-mate pair Illumina libraries. In addition, the genome of *Coprinellus micaceus* was sequenced using Pacific Biosciences platform. Fragment Illumina genomic libraries were produced for 100 ng of DNA was sheared to 270 bp using the Covaris LE220 and size selected using SPRI beads (Beckman Coulter). The fragments were treated with end-repair, A-tailing, and ligation of Illumina compatible adapters (IDT, Inc) using the KAPA-Illumina library creation kit (KAPA biosystems). For long-mate pair libraries (*Crucibulum laeve*, *Dendrothele bispora*, *Heliocybe sulcata*, *Polyporus arcularius* and *Pterula gracilis),* 5 µg of DNA was sheared using the Covaris g-TUBE(TM) and gel size selected for 4 kb. The sheared DNA was treated with end repair and ligated with biotinylated adapters containing loxP. The adapter ligated DNA fragments were circularized via recombination by a Cre excision reaction (NEB). The circularized DNA templates were then randomly sheared using the Covaris LE220 (Covaris). The sheared fragments were treated with end repair and A-tailing using the KAPA-Illumina library creation kit (KAPA biosystems) followed by immobilization of mate pair fragments on strepavidin beads (Invitrogen). Illumina compatible adapters (IDT, Inc) were ligated to the mate pair fragments and 8 cycles or in case of *Heliocybe sulcata* 10 cycles of PCR were used to enrich for the final library (KAPA Biosystems). For *Coprinellus micaceus* unamplified libraries were generated using Pacific Biosciences standard template preparation protocol. 5 µg of gDNA was used to generate each library and the DNA was sheared using Covaris g-Tubes(TM) to generate sheared fragments of >10kb in length. The sheared DNA fragments were then prepared using Pacific Biosciences SMRTbell template preparation kit, where the fragments were treated with DNA damage repair, had their ends repaired so that they were blunt-ended, and 5' phosphorylated. Pacific Biosciences hairpin adapters were then ligated to the fragments to create the SMRTbell template for sequencing. The SMRTbell templates were then purified using exonuclease treatments and size-selected using AMPure PB beads.

All transcriptomes in this study were sequenced using Illumina RNA-Seq. Stranded cDNA libraries were generated using the Illumina Truseq Stranded RNA LT kit. mRNA was purified from 1 µg of total RNA using magnetic beads containing poly-T oligos. mRNA was fragmented and reversed transcribed using random hexamers and SSII (Invitrogen) followed by second strand synthesis. The fragmented cDNA was treated with end-pair, A-tailing, adapter ligation, and 10 cycles or in case of *Coprinopsis marcescibilis*, *Crucibulum leave* and *Pluteus cervinus* 8 cycles of PCR.

The prepared Illumina libraries were quantified using KAPA Biosystem's next-generation sequencing library qPCR kit and run on a Roche LightCycler 480 real-time PCR instrument. The quantified libraries were then multiplexed with other libraries, and the pool of libraries was then prepared for sequencing on the Illumina HiSeq sequencing platform utilizing a TruSeq paired-end cluster kit, v4, and Illumina's cBot instrument to generate a clustered flow cell for sequencing. Sequencing of the flow cell was performed on the Illumina HiSeq2500 sequencer using HiSeq TruSeq SBS sequencing kits, v4, following a 2x150 indexed run recipe. In the case of *Coprinellus micaceus*, *Dendrothele bispora*, *Peniophora* sp. and *Polyporus arcularius* TruSeq paired-end cluster kit, v3 and TruSeq SBS sequencing kits, v3 were used and in the cases of *Crucibulum laeve*, *Heliocybe sulcata* and *Pterula gracilis* 2x100 indexed run recipe was performed.

For PacBio sequencing primer was annealed to the SMRTbell templates and Version P5 sequencing polymerase was bound to them. The prepared SMRTbell template libraries were then sequenced on a Pacific Biosciences RSII sequencer using Version C3 chemistry and 1x240min sequencing movie run times.

4.2   Assembly and annotation—Genomic reads from each pair of Illumina libraries were QC filtered for artifact/process contamination and assembled together with AllPathsLG v. R4940349. Illumina reads of stranded RNA-seq data were used as input for *de novo* assembly of RNA contigs and assembled into consensus sequences using Rnnotator (v. 3.4)50. The Pacific Biosciences sequence data were filtered with smrtanalysis assembled together with Falcon version 201408251, improved with finisherSC52, and polished with Quiver. All genomes were annotated using the JGI Annotation Pipeline and made available via the JGI fungal portal MycoCosm53. Genome assemblies and annotation were also deposited at DDBJ/EMBL/GenBank.

5   Phylogenomic analysis of 104 Agaricomycotina

5.1   Phylogenomic analysis—The genome sequences of 104 species (Supplementary Table 1) were included in the phylogenomic analysis of Agaricomycotina. Two representatives of Tremellomycetes (*Tremella mesenterica* (Treme1), *Cryptococcus neoformans* var. *grubii* H99 (Cryne_H99_1)) were used as outgroups.

We performed all-versus-all blast using mpiBLAST 1.6.054 with default parameters, then identified gene families using the Markov clustering algorithm MCL 14-13755 with an inflation parameter of 2.0. We first identified gene families that contained 52-208 genes (50-200% of the species included in the study), then performed multiple sequence alignment using PRANK 14060347. Ambiguously aligned regions were removed from the alignments using Gblocks 091b56 with the settings -p=yes -b2=26 -b3=10 -b4=5 -b5=h -t=p -e=.gbl. Next, we screened for gene families that contained a single representative gene for each species, or ones that contained inparalogs but no deep paralogs. Deep paralogs were identified following Nagy et al.57. Gene trees were inferred using the PTHREADS version of RAxML 8.1.258 using the PROTGAMMAWAG model and the standard algorithm. A single inparalog, closest to the root based on root-to-tip patristic distances was retained for

each species. Gene families in which >=75% of the species were represented were concatenated into a supermatrix.

We used RAxML 8.1.2 to perform ML analysis and bootstrapping on the concatenated dataset, under a WAG model with gamma-distributed rate heterogeneity partitioned by gene. We ran 100 bootstrap replicates using the rapid hill-climbing algorithm. Because in initial analyses *Peniophora* sp*., Tubaria furfuracea, Clavaria fumosa* were placed on long terminal branches, we performed the following steps to clean the alignments of overly divergent sequences (either due to sequencing errors or pseudogenes). We screened all individual gene trees and excluded proteins with a terminal branch length >2.75 times longer than the average branch length of the gene tree. Altogether 1,294 (in 542 gene families) protein sequences were excluded from the analyses.

5.2   Sensitivity analysis—The robustness of the dataset was tested by eliminating incrementally higher numbers of fast-evolving sites using six levels of stringency in Gblocks 091b56. Using these parameters, we eliminated 8.5% (-b1=78 -b2=78 -b3=10 -b4=10), 24.3% (-b1=78 -b2=78 -b3=8 -b4=15), 36.7% (-b1=88 -b2=88 -b3=8 -b4=15), 46.4% (-b1=95 -b2=95 -b3=8 -b4=15), 50.1% (-b1=100 -b2=100 -b3=8 -b4=15) and 55.2% (-b2=104 -b3=5 -b4=20) of the least reliably aligned regions of the alignments, resulting in trimmed concatenated datasets with 129,886, 107,496, 89,732, 76,153, 70,862 and 63,309 amino acid sites, respectively. We performed ML phylogenetic inference for each of the reduced datasets in RAxML as described above.

6   Maximum Likelihood analyses of the 5,284-taxon dataset

Maximum likelihood trees for the 5,284-taxon dataset were inferred using the parallel version of RAxML 8.1.258 under the GTR model with gamma distributed rate heterogeneity (4 categories) with three partitions corresponding to the LSU*, ef1-α* and *rpb2* loci. The phylogenomic tree was used as a backbone monophyly constraint. We performed 245 ML inferences and tested whether these trees adequately represented the plausible set of topologies given the alignment. This was done to ensure that phylogenetic uncertainty is properly taken into account in subsequent comparative analyses. If our tree set contains all plausible topologies, then the rolling average of pairwise Robinson-Foulds (RF) distances should show a saturation as a function of increasing the number of trees. To this end, we computed RF distance for each pair of trees for incrementally larger numbers of trees using R package "phangorn" v.2.0.259. We then plotted the rolling average, maximum and minimum values as a function of the number of trees in R.

7   Molecular clock dating of the 5,284-taxon dataset

Due to computational limitations, we focused on 10 ML trees that maximize topological diversity (as inferred based on RF distances) as representative trees for molecular clock analysis. These were chosen by first calculating pairwise RF distances between trees, then hierarchically clustering trees using Ward's clustering method (as implemented in the hclust R function). The ten ML trees for subsequent analyses were chosen evenly from the resulting clusters of trees. To overcome the computational limitations of inferring accurate chronograms for thousand-tip phylogenies, we adopted a two-step strategy. First,

PhyloBayes 4.1b60 was used to infer parameters of a birth-death model and divergence times of trees on 10% subsampled versions of the 5,284-taxon dataset. Subsampled datasets were obtained by randomly deleting 90% of the species, but forcing key descendants of fossil-calibrated nodes to be retained in the subsampled alignments. Then we used the ages and parameters estimated in PhyloBayes as input parameters for FastDate development version61 (provided by Thomas Flouri, downloaded Jan 5 2017) for analyzing the complete 5,284-species dataset.

PhyloBayes analyses were run using the 10% subsampled dataset, a birth-death prior on divergence times, an uncorrelated gamma multiplier relaxed clock model and a CAT-poisson substitution model with a gamma distribution on the rate across sites. A uniformly distributed prior was applied to fossil calibration times. All analyses were run until convergence, typically 15,000 cycles. Convergence of chains was assessed by visually inspecting the likelihood values of the trees and the tree height parameter. We sampled every tree from the posterior and after discarding the first 7,000 samples as burn-in we summarized the posterior estimates using the *readdiv* function of PhyloBayes.

Next, we used FastDate, a program that implements the speed dating algorithm described in Akerborg et al.61. FastDate was run on the complete trees (5,284 species) with the node ages constrained to the values of the 95% highest posterior densities of the ages inferred by PhyloBayes. FastDate analyses were run with time discretized into 1,000 intervals and the ratio of sampled extant individuals set to 0.14.

8 Fossil calibrations

The extensive sampling density of our tree allowed us to use more fossil calibration points than any study before and to place them more precisely within the tree. Eight fossils were used as calibration points (Supplementary Table 2) for the crown node of the specified taxa.

We excluded a number of prospective well-preserved fossils for reasons of redundantly calibrating an already calibrated node (*Appianoporites vancouverensis* – Hymenochaetales62, *Protomycena electra* – marasmioid clade63, *Cyathus dominicanus* – Nidulariaceae64, *Fomes idahoensis* – Polyporales65. *Geastrum tepexensis* 66 was not considered as it could be assigned to either of the two earth-star clades, one in the Phallomycetidae (Geastraceae) or the other in the Boletales (*Astraeus*). For other mushroom fossils, the taxonomic affiliations were deemed too uncertain.

To investigate if there is any conflict between the fossil calibration points we conducted a fossil cross-validation analysis following Near et al.67. For this, we ran PhyloBayes analyses on one of the 10% subsampled trees with the same settings as mentioned above, using a single fossil calibration point at a time. This resulted in eight independent molecular dating analyses. To quantify conflict between single fossil calibrations, first we calculated the sum of the square differences between molecular age estimates (MA) and fossil ages (FA):

$$SS_x = \sum_{i \neq x} D_i^2$$

where x is the fossil calibration point used and D_i is the difference between MA and FA for fossil *i*. We ordered the *SS* values of each of the eight analyses in descending order and calculated the average squared deviation for all fossil calibrations:

$$S = \frac{\sum_{x=1}^{n} \sum_{i \neq x} D_i^2}{n(n-1)}$$

Next, the analysis with the highest *SS* value was removed and *s* was recalculated. We continued this process until only two analyses remained. In parallel, we performed one-tailed F-tests to check if the removal of the fossil had a significant effect on the variance of *s*. The principle of this procedure is that during the stepwise removal of fossils *s* should decrease by small constant values and variance should not decrease significantly.

9   Genome-based molecular clock analyses

We examined the robustness of our molecular age estimates using phylogenomic methods as an alternative to the 5,284 species phylogeny. Specifically, we tested whether the differences between our and previous[17,18] molecular clock estimates for Agaricomycete orders were attributable to differences in the dataset or analytical method used or a difference in how precisely fossils could be placed on the tree. To this end, we performed a series of molecular clock analyses on our phylogenomic dataset that resembled that of Kohler and Floudas in terms of topology and taxon sampling density, but differed in the placement of some fossil calibrations. A key difference was that our phylogenomic tree included the most recent common ancestor (mrca) of the Hymenochaetales and that of the Suillaceae, which allowed us to calibrate the MRCA of these clades, as opposed to their stem nodes by Kohler et al and Floudas et al. Further, our analysis includes the MRCA of the Nidulariaceae, a relatively recent node which can be calibrated by two well-preserved fossils described recently[64].

9.1   Phylogenomic dataset—We used a smaller, more conserved subset of the 568-gene and 104-species phylogenomic dataset (which was computationally not tractable in these analyses). First, we selected the first 70 most conserved genes of the 568-gene dataset by calculating the mean genetic distances for each gene using the dist.alignment function of the seqinR R package v.3.4-568. To enable a more accurate placement of fossil calibration points we added additional three species (*Cyathus striatus*, *Pycnoporus cinnabarinus*, *Suillus brevipes*) to this dataset (Supplementary Table 1) and excluded two taxa that harbored ambiguous positions. We searched homologous sequences in the additional genomes using blastp v.2.7.169 with one randomly selected gene from each of the 70 gene families as query. We selected the best hit (smallest E-value) as a 1-to-1 ortholog if the second best hit had a significantly worse E-value (by 20 orders of magnitude). Protein clusters were aligned by PRANK v.10080246,47 using default settings. Next, conserved blocks of the alignments were selected using Gblocks V.0.91b56 with default settings except for the minimum length of a block which was set to 5 and gap positions in half of the sequences were allowed. A phylogenomic tree was constructed by RAxML v.8.2.1158 under WAG+G substitution model partitioned by gene.

9.2 Calibrations—To dissect sources of differences in molecular age estimates, we ran analyses under 3 fossil calibration schemes (Supplementary Data 2) and the 105-species phylogenomic tree. First we used the same fossil calibration scheme as for the 5,284-species phylogenetic dataset ("Default calibration scheme"). Next, we replicated the analyses of Kohler et al.18 on our tree, using the fossil calibration points from Kohler et al. ("Kohler et al. calibration scheme 1"). For this, we placed the suilloid ectomycorrhiza fossil in the split of Suillinae/Paxillinae/Sclerodermatinae and *Archaeomarasmius leggettii* in the mrca of *Gymnopus luxurians* and *Schizophyllum commune* with uniformly distributed 40–60 mya and 70–110 mya time priors, respectively. Finally, we used the calibrations used by Kohler et al. (2) but placed the two fossils in the mrca-s of the Suillaceae and marasmioid clade, respectively (Kohler et al.18 calibration scheme 2"). In all analyses we constrained the age of the root to be between 300 mya and 600 mya.

9.3 Penalized likelihood analysis in r8s—We ran a series of molecular clock analyses in r8s v.1.8170. A cross-validation analysis was performed to determine the optimal smoothing parameter (λ) by testing values across 7 orders of magnitude starting from 10^{-3}. The additive penalty function was applied and the optimization was run 25 times starting from independent starting points. In one optimization step, after reaching an initial solution, the solution was perturbed and the truncated Newton (TN) optimization was rerun 20 times. We compared the results of previous studies to that of analyses across seven ancestral nodes in Agaricomycotina (Supplementary Data 2).

9.4 Bayesian molecular clock dating—We used the mcmctree method implemented in PAML version 4.8a71. The independent-rates clock model, a WAG substitution model and approximate likelihood calculation72 were used. The birth rate, the death rate and the sampling fraction of the birth-death process were set to 1, 1 and 0.14 respectively. The shape and the concentration parameter of the gamma-Dirichlet prior for the drift rate coefficient ($\sigma2$) was set to 1 and three different scale parameters were tested (10, 100, 1,000) to see their effect on the time estimates. The substitution rates of each gene were estimated by codeml under a global clock model, to set the parameters of the gamma-Dirichlet prior for the overall rate. By calculating the mean substitution rate of the loci and examining the density plot of the rates we set up a prior which reasonably fitted the data: the shape parameter, the scale parameter and the concentration parameter were set to 5, 90.7441 and 1, respectively, resulting in an average substitution rate per site per time unit of 0.055. We set the time unit to 100 myr and applied uniform priors on 8 fossil calibrations with lower and upper hard bounds. MCMC (Markov chain Monte Carlo) analysis was run for 80,000 iterations, discarding the first 20,000 iterations as a burn-in and sampling every 30th tree from the posterior. After three independent analyses were run the convergence of log-likelihood values was visually inspected and the estimated ages were compared between replicates.

10 Analyses of diversification and character evolution

10.1 Character coding—We discretely coded three characters, the presence of a cap, fruiting body type and substrate preference for the 5,284 species. Fruiting body types were coded as one of six types and data were compiled from the literature. The six character states

distinguished were: 0 – no fruiting body; 1 – resupinate; 2 – agaricoid; 3 – cyphelloid; 4 – gasteroid/secotioid; 5 – coralloid/clavarioid. Transitional morphologies, or species for which no clear decision could be made on fruiting body type were coded as uncertain. Resupinate fruiting bodies were defined as crust-like or effused, flat morphologies that follow the morphology of the substrate, but irrespective of thickness or hymenophore type. The agaricoid type was defined as having a distinguishable stipe and cap. Cyphelloid species were coded following Bodensteiner73. The gasteroid types included species with closed fruiting bodies that produce spores internally. No distinction was made between secotioid, sequestrate and false-truffle morphologies and all were coded as gasteroid. Fruiting bodies with club-shaped or branched, erect morphology but no differentiated cap were considered coralloid/clavarioid.

The presence of a cap, i.e. pileate-stipitate morphology, was coded based on literature data as either absent (state 0) or present (state 1). Species with rudimentary or reduced caps were coded as uncertain.

We coded species' preference for substrate based on literature data (detailed listing of resources used is not given) as either gymnosperm, angiosperm, or both (i.e. generalist species). Species were considered gymno- or angiosperm specialists if >90% of records were for either plant group, or their habitat preferences in taxonomic literature were described by the terms 'exclusively', 'predominantly', 'mostly', or occurring on the least dominant substrate 'rarely', 'very rarely' or 'exceptionally'. On the other hand, species having records on both gymno- and angiosperm substrates, or described in the literature as generalists, or given multiple gymno- or angiosperm substrate plant species were coded as generalists. Species with insufficient data or no data at all were treated as missing data. Soil-inhabiting saprotrophs were coded based on their association with either gymno- or angiosperms, if a clear preference was reported in the literature.

10.2 Tests of the Latitudinal Diversity Gradient Hypothesis

10.2.1 Global positioning system data: We downloaded 5,884,445 fungal GPS records from the GBIF database, representing 4,429 Agaricomycetidae species. For 848 species, a location based on the province, country, and/or biogeographic realm74 was obtained from the literature. In cases where only the province, country or biogeographic realm was available, we took the centroid of the area as a proxy for GPS location. All GPS data were handled and processed in R75. Noise was added to identical GPS coordinates using the *jitter* function in R.

10.2.2 Analyses of geographic diversification: State-dependent diversification rates were estimated in two ways: (1) using centroid latitudes as continuous traits (e.g. Sánchez-Ramírez et al.35), and (2) using discrete areas. We used the data mentioned above to first calculate a centroid coordinate (RGEOS R package) in cases were multiple GPS records exist per species. Then we took the centroid latitude for each species. For singletons, we simply took the latitude of each record. We also used the GPS database to calculate a standard deviation for latitude per species. For species with a single record, we took the mean standard deviation of species with multiple records. We fitted multiple Quantitative

State Speciation and Extinction (QuaSSE[76]) models, using a maximum-likelihood approach, to ten of the 5,284-species chronograms. Models included speciation rate changes as a constant function of the trait (no effect), as a linear function, or as a Gaussian function, keeping the extinction rate constant[76]. We also added two models in which the extinction rate varied as linear or Gaussian functions, while speciation rate remained constant. To improve the efficiency of the algorithm given the scale of the tree, we applied the following settings to the models: method="fftC", dt.max=1 and nx=256. Akaike information criterion (AIC) values were averaged across phylogenies and compared between different models. We used the best supported model to interpolate speciation rates into a 1 x 1 degree global map made with Natural Earth. Free vector and raster map data @ naturalearthdata.com.

To obtain discrete areas, first we divided all terrestrial WWF ecoregions into either tropical or extra-tropical. For tropical areas we considered: Tropical & Subtropical Moist Broadleaf Forests, Tropical & Subtropical Dry Broadleaf Forests, Tropical & Subtropical Grasslands, Savannas & Shrublands. All other terrestrial ecoregions were deemed extra-tropical. Ecoregion polygons were integrated (i.e. dissolved) in a way that only two-state areas were found (Supplementary Note 7). For species with multiple GPS records, we extracted binary information about their presence in both areas. For records that were not found precisely within the geometry of the area, we took the area to which the distance to the GPS point was closer. To assign discrete states to each species with multiple records, our criterion was to assign a "widespread" state (both areas) if records for the area with the minor frequency was higher than 0.2. In any other case, we assigned "tropical" or "extra-tropical" states to taxa in the area with the highest frequency. For taxa that had only biogeographic realm data, we coded them as follows: "widespread": Neotropical, Afrotropical, Oceanian/Australia; "tropical": Panamenian, Oriental; and "extra-tropical": Europe/Palearctic/North Asia, Nearctic, Saharo-Arabian, Sino-Japanese. Using these three states for each taxon, we fitted multiple constrained models and one full model of Geographic State Speciation and Extinction (GeoSSE[77]) in a maximum-likelihood framework. The full model (a) consisted of seven parameters: (1) speciation rate in the tropics, (2) speciation rate in the extra-tropical zone, (3) the allopatric speciation rate (speciation rate in both tropical and extra-tropical regions), (4) extinction rate in the tropics, (5) extinction rate in the extra-tropical zone, and dispersal rates to (6) the tropics and to (7) the extra-tropical zone. The constrained models consisted of: (a) speciation in the tropics is equal to speciation in the extra-tropical zone; (b) extinction in the tropics is equal to extinction in the extra-tropical zone; (c) dispersal to the tropics occurs at the same rate as dispersal to the extra-tropical zone. In each case, a single parameter for speciation, extinction, and dispersal was respectively estimated, allowing the other parameters of the model to vary. To explore the parameter space better, we re-estimated parameters using MCMC on the full model. In a similar way as above, we used AIC scores to rank the models.

10.3 Analyses of character evolution

10.3.1 Model tests: To infer substitution models that best describe the evolution of agaricoid/non-agaricoid fruiting bodies we used ML and MCMC approaches implemented in BayesTraits 2.0 Linux 64 Quad Precision alternative build[78] and the R package diversitree v.0.9-83[9]. The Binary State Speciation and Extinction (BiSSE) model[38] was

used in diversitree. We performed model tests by first constraining the forward and reverse transition rates between non-agaricoid (state 0) and agaricoid type (state 1) to be equal (q_{01} = q_{10}). We also separately constrained each of the rates to be zero ($q_{01} = 0$ or $q_{10} = 0$). Each of the constrained models were compared to the best fit model based on log-likelihood values (ML analyses in BayesTraits), log Bayes factors (MCMC analyses in BayesTraits) or likelihood ratio test and Akaike information criterion scores (ML analyses of BiSSE model in diversitree)[38,39,78,79]. In BayesTraits, a difference of 2.00 log likelihood units (ML approach) or a difference of 10 log marginal likelihood units (MCMC approach) was considered as significant support for a model over another, while in the BiSSE analyses significance was assessed using likelihood ratio tests ($p < 0.05$).

10.3.2 *BayesTraits* **analysis:** BayesTraits analyses (ML and MCMC) were performed on 245 phylogenetic trees using the MultiState module of the program. Before the final MCMC analyses, we tried several prior distributions (uniform, exponential, gamma and the hyper-prior versions of these) with different settings. Based on preliminary analyses we found that the gamma distribution was most optimal, therefore in further analyses we used a gamma hyper-prior with different prior distributions for each parameter (Supplementary Note 5). All preliminary BayesTraits analyses were conducted with the following settings: 1,010,000 generations, 10,000 generations as burn-in and sampling every 500th generation. We forced Markov chains to spend 200,000 generations on each tree using the *equaltree* option, with 100,000 generations as burn-in and sampling every 500th generation. The marginal likelihood was estimated by the stepping stone method[78,80] using 50 stones with a chain length of 5,000. All analyses in BayesTraits were repeated three times to check the congruence of independent runs.

10.3.3 *Diversitree* **analysis:** We used 10 chronograms to analyse trait dependent diversification under the binary state speciation and extinction (BiSSE) model implemented in the R package diversitree v.0.9-103[38,39]. Maximum likelihood search started from the point in the parameter space determined by the function *starting.point.bisse*. Bayesian MCMC was performed using an exponential prior, defined as $1/(2r)$, where r is the character independent diversification rate. State specific sampling fractions were defined based on data from Species Fungorum[44] (see below: Accounting for non-random incomplete taxon sampling). We first optimized the MCMC sampler's step size argument by running 100 generations, then we ran MCMC analyses for 20,000 generations with burn-in set to 10%. The convergence of the chains was visually checked based on likelihood and parameter values.

10.4 Ancestral character state reconstruction—We reconstructed the ancestral states using stochastic character mapping as implemented in *phytools* v.06-208[1], to reveal the dynamics of fruiting body types and substrate preference through time. This method is a modified version of a previously published algorithm[82], which samples discrete character histories from the posterior probability distribution. We performed the analysis with the *make.simmap* function on 10 time calibrated trees under a Markov model with all rates different (ARD). The stochastic character histories were simulated 5,000 times. We plotted state posterior probabilities through time using a custom R script. Briefly, we summarized

character state posterior probabilities through the time scale of our 10 chronograms split into 100 bins. The plot was created using *ggplot* and *geom_area* functions of ggplot2 v.2.2.183. Ancestral probability distributions of substrate preference for the mrca-s of each of the orders and some additional clades were plotted as pie charts using the *nodelabels* function of *ape* v.4.1.84.

10.5   Diversification rate analyses

10.5.1   Accounting for random and incomplete taxon sampling: To meet the assumption of random or complete sampling of the BAMM and BiSSE models[20,39], we specified the sampling fraction of each genus in accordance with the described number of species based on Species Fungorum[44]. To gather information on described species, we screened all orders of the Agaricomycetes, Dacrymycetes and Tremellomycetes in Species Fungorum and gathered all species with a custom java program (available from the authors upon request). We took into account taxonomic and nomenclatural synonymy if indicated by Species Fungorum. We accounted for incomplete taxon sampling by two strategies. First, we assigned specific sampling fractions to the character states (BiSSE model) or to genera (BAMM model). In these cases we used the built-in correction of the BiSSE and BAMM models[20,85] to account for missing species in our phylogeny. Second, because we could have unintentionally oversampled certain genera, (e.g. because of better availability of specimens), we statistically tested for oversampling and generated a pruned phylogeny in which each genus is represented in proportion of its described diversity. We adjusted taxon sampling in our phylogeny by iteratively deleting species from genera that were oversampled relative to the mean sampling fraction of the tree, until sampling fractions of each genera corresponded their known size as judged by a comparison to Species Fungorum. To do this we performed a hypergeometric test ($p<0.05$) at each iteration of species removal. Elimination of species was stopped when oversampling disappeared ($p>0.05$, hypergeometric test). With this procedure we wanted to produce a 'skeletal tree' (Sensu FitzJohn et al.[85]), where species were both evenly and randomly sampled from every genera[85].

10.5.2   Trait-dependent diversification rate analyses: We performed analyses under the BiSSE model to examine the effect of agaricoid fruiting body type on diversification rate. BISSE analyses were carried out in diversitree v.09-10 as described above, with the following differences. We performed model tests to examine if the presence of a cap influenced speciation and extinction rates. To this end, we first constrained state-specific speciation or extinction rates to be equal ($\lambda_0 = \lambda_1$ or $\mu_0 = \mu_1$) then constrained both the speciation rates and extinction rates to be equal ($\lambda_0 = \lambda_1$ and $\mu_0 = \mu_1$). Models were compared by likelihood ratio test (LRT) in R.

10.5.3   Trait-independent diversification rate analyses: We used BAMM 2.5.0. (Bayesian Analysis of Macroevolutionary Mixtures)[20], to examine rate heterogeneity across lineages and detect shifts in diversification rates. We analyzed 10 chronograms and ran MCMC analyses for 100 million generations using four independent chains per analysis with 50 million generations as burn-in. Prior parameters were optimized using the *setBAMMpriors* function in BAMMtools 2.1.6.86, except for the prior on the expected

number of shifts, which was set to 270 based on preliminary runs. We accounted for incomplete taxon sampling as described above. We checked the convergence of chains by visually inspecting the convergence of likelihoods, by calculating the effective sample size (ESS) and the Geweke's diagnostic87 of log-likelihoods, numbers of shifts and evolutionary rate parameters, using functions in CODA 0.19-188. Geweke's diagnostic tests for the quasi equality of the means of parameters sampled at different parts of the MCMC analysis; if means at the beginning and end regions of the post-burn-in MCMC sample do not differ to a statistically significant extent (P>0.05), then the Markov chain is considered to be in stationary phase. To ensure that a shift is highly supported by the data and the prior had negligible contribution, we examined only core shifts, i.e. those with a prior-to-posterior marginal odds ratio exceeding 586.

We compared core shifts across 10 chronograms to obtain a consensus view on shifts that can be detected in all or most of the trees. To this end, we first empirically identified taxonomically similar clades for which a core shift was inferred, taking into account topological differences among trees. Then we noted whether the mean diversification rate change after the shift is positive or negative (i.e. rate acceleration or deceleration). There were cases when several core shifts were inferred on adjacent branches around the mrca of a given clade. These come from distinct shift configurations sampled during the MCMC analysis and correspond to the same signal of rate variation in the data but were located to adjacent branches of the tree. In such cases, we chose the shift with the highest posterior probability, noting that the biological reality of increasing rates might be spread out across a few adjacent branches around the one with the highest posterior. Finally, shifts were referred to as congruent core shifts if they were highly congruent across >=4 trees and had strong tree support (mean posterior probability > 0.5).

Next, we assessed whether posterior probabilities of congruent core shifts reached convergence in a fashion similar to the 'cumulative' function of AWTY89. For this, we calculated the posterior probability of each core shift at each generation, as if the analysis was stopped at that point and plotted posterior probabilities as a function of generation using the ggplot2 v.2.2.1 package83. We also took into account the distinct shift configurations by examining whether a rate increase, after a congruent core shift was explained by a rate decrease after another core shift. First, we determined congruent core shift - core shift pairs which could potentially be mutually exclusive to each other. These shift pairs were determined in one tree, usually in the tree where a congruent core shift had high posterior probability. Then we calculated two kinds of posterior proportions: one for co-occurring shift pairs and one for each of the single occurrence of the shifts. We said that two shifts were mutually exclusive to each other if only a negligible co-occurrence was presented and the direction of the diversification rate change was different between the single occurrence posterior samples.

To reveal tree-wide evolutionary patterns we calculated average net rates through time using the *getRateThroughTimeMatrix* function and plotted by the *plotRateThroughTime* function of the BAMM package.

10.5.4 Validation of BAMM estimates: There have been critics of the BAMM method recently[90,91]. Meyer and Wiens[91] found that the method-of-moments estimator (MS) yielded stronger relationship between true and estimated diversification rates than BAMM, particularly in smaller clades. Therefore to validate the BAMM results we used the method-of-moments estimator (MS) on clades with congruent core shifts. The MS approach estimates diversification rates from species richness and clade age while it can incorporate incomplete taxon sampling and extinction rate by assuming a relative extinction fraction (ε = extinction rate / speciation rate)[92]. We used the *bd.ms* function in *geiger 2.0.6*[93]. The analyses were performed on all the 85 clades with congruent core shifts, using three different relative extinction fractions (0, 0.45, 9) and calculating with both stem and crown ages. We calculated unsampled species fractions using the genus-specific sampling fractions we determined for BAMM analyses. For the same set of clades we calculated average net diversification and net speciation rates from BAMM data using the *getCladeRates* function. Then we performed linear regressions between MS estimates with different settings and average net diversification or net speciation rates from BAMM. We examined the adjusted R-squared and the p-values of the models to evaluate the correspondence between the two methods.

10.6 Detecting Mass Extinction Events—We performed analyses using the compound Poisson process (CPP) on mass extinction times model (CoMET)[27,94], to examine tree-wide variation in diversification rate and occurrence of mass extinctions during the evolution of mushroom-forming fungi. First, we conducted a model comparison on ten chronograms using the CoMET model with a constant rate birth-death process implemented in the TESS 2.1.0. R package[95]. We compared models with and without mass extinction events based on marginal likelihoods. We allowed the occurrence of a mass extinction event along the entire time span of a tree and we set the survival probability of species to 0.1 (corresponding to 10% of the species surviving a mass extinction event). The overall sampling fraction of species was set to 0.14. MCMC analyses were run for 20,000 generations and the first 2,000 posterior samples were discarded as a burn-in. Marginal likelihoods were estimated using stepping stone simulation using 100 stepping stones.

Then, we performed reversible jump Markov Chain Monte Carlo (rjMCMC) analyses under the CoMET model to sample from the space of episodically varying birth-death processes with mass-extinction events. In this analysis, we also tested the significance of the occurrence of a mass extinction event by performing model tests within time intervals. Bayes factor values BF > 10 or lnBF > 6 were considered strong support for a model, following Höhna et al.[96] and Kass & Raftery[97]. We examined the sensitivity of the posterior probabilities to different prior settings in preliminary analyses of a randomly chosen tree. We examined models with 2 or 10 expected mass extinction events, with 30, 100 or 270 expected rate changes and with survival probabilities of 0.001, 0.05 or 0.3. All of these preliminary analyses were run for 1.6 million generations with 100,000 generations as burn-in. We used a log-normal prior on speciation and extinction rates with a mean of 0.2 and 0.15 and a standard deviation of 0.5 and 0.5, respectively. In the final analyses we used all 10 chronograms and an empirical hyperprior on rate parameters based on 200,000 iterations with 100,000 burn-in. The priors on the number of expected mass extinction and

the expected rate changes were set to 2 and 30 respectively, based on results of preliminary analyses. We set the survival probability to 0.05. Analyses were run for 3 million generations with 1 million generations as burn-in. The convergence of the analyses was checked by visually inspecting the log likelihood values and by computing the effective sample size and the Geweke diagnostic for the log likelihoods, the number of speciation rate shifts, the number of extinction rate shifts and the number of mass extinction events using the *effectiveSize* and the *geweke.diag* function of the *CODA* 0.19.-1 package[88], respectively. To check the convergence of interval-specific parameters we used the *tess.plot.singlechain.diagnostics* function of the *TESS* package.

Supplementary Material

Refer to Web version on PubMed Central for supplementary material.

Authors

Torda Varga[1], Krisztina Krizsán[1], Csenge Földi[1], Bálint Dima[2], Marisol Sánchez-García[3], Santiago Sánchez-Ramírez[4], Gergely J. Szöll si[5], János G. Szarkándi[6], Viktor Papp[7], László Albert[8], William Andreopoulos[9], Claudio Angelini[10,11], Vladimír Antonín[12], Kerrie W. Barry[9], Neale L. Bougher[13], Peter Buchanan[14], Bart Buyck[15], Viktória Bense[1], Pam Catcheside[16], Mansi Chovatia[9], Jerry Cooper[17], Wolfgang Dämon[18], Dennis Desjardin[19], Péter Finy[20], József Geml[21], Sajeet Haridas[9], Karen Hughes[22], Alfredo Justo[3], Dariusz Karasi ski[23], Ivona Kautmanova[24], Brigitta Kiss[1], Sándor Kocsubé[6], Heikki Kotiranta[25], Kurt M. LaButti[9], Bernardo E. Lechner[26], Kare Liimatainen[27], Anna Lipzen[9], Zoltán Lukács[28], Sirma Mihaltcheva[9], Louis N. Morgado[21,#], Tuula Niskanen[27], Machiel E. Noordeloos[21], Robin A. Ohm[29], Beatriz Ortiz-Santana[30], Clark Ovrebo[31], Nikolett Rácz[6], Robert Riley[9], Anton Savchenko[32,&], Anton Shiryaev[33], Karl Soop[34], Viacheslav Spirin[32], Csilla Szebenyi[6,&&], Michal Tomšovský[35], Rodham E. Tulloss[36], Jessie Uehling[37], Igor V. Grigoriev[9,38], Csaba Vágvölgyi[6], Tamás Papp[6,&&], Francis M. Martin[39], Otto Miettinen[32], David S. Hibbett[3], and László G. Nagy[1,*]

Affiliations

[1]Synthetic and Systems Biology Unit, Biological Research Centre, Hungarian Academy of Sciences, H-6726 Szeged, Hungary [2]Department of Plant Anatomy, Institute of Biology, Eötvös Loránd University, Pázmány Péter sétány 1/C, H-1117 Budapest, Hungary [3]Clark University, Biology Department, 950 Main street, 01610 Worcester, Ma, USA [4]Department of Ecology and Evolutionary Biology, University of Toronto, M5S 3B2, Toronto, Ontario, Canada [5]MTA-ELTE 'Lendület' Evolutionary Genomics Research Group, Department of Biological Physics, Eötvös Loránd University, Pázmány Péter sétány 1/A, H-1117 Budapest, Hungary [6]Department of Microbiology, Faculty of Science and Informatics, University of Szeged, Közép 52, 6726 Szeged, Hungary [7]Department of Botany, Faculty of Horticultural Science, Szent István University, H-1518 Budapest, Hungary [8]Hungarian Mycological Society, P.O. Box 89, H-1300 Budapest Hungary [9]US Department of Energy (DOE) Joint Genome Institute, Walnut Creek, CA, 94598, United States [10]Via Cappuccini,

78, 33170 Pordenone, Italy [11]Jardin Botanico Nacional Ma. Moscoso, Santo Domingo, Dominican Republic [12]Department of Botany, Moravian Museum, Zelný trh 6, 659 37, Brno, Czech Republic [13]Western Australian Herbarium, Science and Conservation, Department of Biodiversity, Conservation and Attractions, Locked Bag 104, Bentley Delivery Centre, WA 6983, Australia [14]Manaaki Whenua – Landcare Research, Private Bag 92170, Auckland 1142, New Zealand [15]Institut de Systématique, Evolution, Biodiversité (ISYEB - UMR 7205), Muséum National d'Histoire Naturelle, Sorbonne Université, CNRS, CP 39, 12 Rue Buffon, F-75005 Paris, France [16]State Herbarium of South Australia, G.P.O. Box 1047, Adelaide, South Australia 5001, Australia [17]Manaaki Whenua – Landcare Research, PO Box 69040, Lincoln 7640, New Zealand [18]Oberfeldstraße 9, A-5113 St. Georgen bei Salzburg, Austria [19]Department of Biology, San Francisco State University, 1600 Holloway Avenue, San Francisco, CA, USA [20]Zsombolyai u. 56., H-8000, Székesfehérvár, Hungary [21]Naturalis Biodiversity Center, Leiden, the Netherlands [22]Department of Ecology and Evolutionary Biology, University of Tennessee, Knoxville, TN, USA [23]Department of Mycology, W. Szafer Institute of Botany, Polish Academy of Sciences, Kraków, Poland [24]Natural History Museum, Slovak National Museum, Vajanského nábr. 2, SK–810 06 Bratislava, Slovakia [25]Finnish Environment Institute, Biodiversity Unit, P.O. Box 140, Helsinki, FI-00251 Finland [26]CONICET - Universidad de Buenos Aires, Instituto de Micología y Botánica (InMiBo), DBBE, FCEN, Ciudad Universitaria Pab. II (1428) Buenos Aires, Argentina [27]The Jodrell Laboratory, Royal Botanic Gardens, Kew, Surrey TW9 3AB, UK [28]Damjanich u. 54, H-1071 Budapest Hungary [29]Department of Biology, Microbiology, Utrecht University, 3584CH Utrecht, The Netherlands [30]Center for Forest Mycology Research, US-Forest Service, Northern Research Station, Madison, USA [31]Department of Biology, University of Central Oklahoma, Edmond, OK 73034, USA [32]Botanical Museum, University of Helsinki, PO Box 7, 00014, Helsinki, Finland [33]Institute of Plant and Animals Ecology, Russian Academy of Sciences, 8 March str. 202, 620144 Ekaterinburg, Russia [34]Swedish Museum of Natural History, Department of Cryptogamic Botany, Box 50007, S-104 05 Stockholm, Sweden [35] Faculty of Forestry and Wood Technology, Mendel University in Brno, Zemedelska 3, 613 00, Brno, Czech Republic [36]Herbarium Rooseveltensis Amanitarum P. O. Box 57, Roosevelt, New Jersey 08555-0057, USA; Res. Assoc. (hons.), the New York Botanical Garden, Bronx, New York [37]Plant and Microbial Biology, University of California, Berkeley, CA 94703, USA [38] Department of Plant and Microbial Biology, University of California Berkeley, Berkeley, CA 94720, United States [39]Institut National de la Recherche Agronomique (INRA), Laboratory of Excellence Advanced Research on the Biology of Tree and Forest Ecosystems (ARBRE), UMR 1136, Champenoux, France

Acknowledgments

References

1. Jetz W, Pyron RA. The interplay of past diversification and evolutionary isolation with present imperilment across the amphibian tree of life. Nat Ecol Evol. 2018; 2:850–858. [PubMed: 29581588]

2. Jetz W, Thomas GH, Joy JB, Hartmann K, Mooers AO. The global diversity of birds in space and time. Nature. 2012; 491:444–448. [PubMed: 23123857]

3. Rabosky DL, et al. Rates of speciation and morphological evolution are correlated across the largest vertebrate radiation. Nat Commun. 2013; 4

4. Alfaro ME, et al. Explosive diversification of marine fishes at the Cretaceous–Palaeogene boundary. Nat Ecol Evol. 2018; 2:688–696. [PubMed: 29531346]

5. Alfaro ME, et al. Nine exceptional radiations plus high turnover explain species diversity in jawed vertebrates. Proc Natl Acad Sci U S A. 2009; 106:13410–4. [PubMed: 19633192]

6. Nagy LG, et al. The evolution of defense mechanisms correlate with the explosive diversification of autodigesting coprinellus mushrooms (agaricales, fungi). Syst Biol. 2012; 61:595–607. [PubMed: 22223448]

7. Wilson AW, Hosaka K, Mueller GM. Evolution of ectomycorrhizas as a driver of diversification and biogeographic patterns in the model mycorrhizal mushroom genus Laccaria. New Phytol. 2017; 213:1862–1873. [PubMed: 28164331]

8. Wilson AW, Binder M, Hibbett DS. Diversity and evolution of ectomycorrhizal host associations in the sclerodermatineae (Boletales, Basidiomycota). New Phytol. 2012; 194:1079–1095. [PubMed: 22471405]

9. Sánchez-Ramírez S, Tulloss RE, Amalfi M, Moncalvo JM. Palaeotropical origins, boreotropical distribution and increased rates of diversification in a clade of edible ectomycorrhizal mushrooms (Amanita section Caesareae). J Biogeogr. 2015; 42:351–363.

10. Sánchez-Garcia M, Matheny PB. Is the switch to an ectomycorrhizal state an evolutionary key innovation in mushroom-forming fungi? A case study in the Tricholomatineae (Agaricales). Evolution (N. Y). 2017; 71:51–65.

11. Wilson AW, Binder M, Hibbett DS. Effects of gasteroid fruiting body morphology on diversification rates in three independent clades of fungi estimated using binary state speciation and extinction analysis. Evolution (N. Y). 2011; 65:1305–1322.

12. Hibbett DS. After the gold rush, or before the flood? Evolutionary morphology of mushroom-forming fungi (Agaricomycetes) in the early 21st century. Mycol Res. 2007; 111:1001–1018. [PubMed: 17964768]

13. Hibbett DS. Trends in morphological evolution in homobasidiomycetes inferred using maximum likelihood: A comparison of binary and multistate approaches. Syst Biol. 2004; 53:889–903. [PubMed: 15764558]

14. Hibbett DS, Binder M. Evolution of complex fruiting-body morphologies in homobasidiomycetes. Proc Biol Sci. 2002; 269:1963–1969. [PubMed: 12396494]

15. Matheny PB, et al. Major clades of Agaricales: a multilocus phylogenetic overview. Mycologia. 2006; 98:982–95. [PubMed: 17486974]

16. Kirk, P, Cannon, P, Minter, D, S, J. Dictionaty of the Fungi. CABI International; 2011.

17. Floudas D, et al. The Paleozoic Origin of Enzymatic Lignin Decomposition Reconstructed from 31 Fungal Genomes. Science (80-.). 2012; 336:1715–1719.

18. Kohler A, et al. Convergent losses of decay mechanisms and rapid turnover of symbiosis genes in mycorrhizal mutualists. Nat Genet. 2015; 47:410–415. [PubMed: 25706625]

19. Lutzoni F, et al. Contemporaneous radiations of fungi and plants linked to symbiosis. Nat Commun. 2018; 9

20. Rabosky DL. Automatic detection of key innovations, rate shifts, and diversity-dependence on phylogenetic trees. PLoS One. 2014; 9

21. McKenna DD, Sequeira AS, Marvaldi AE, Farrell BD. Temporal lags and overlap in the diversification of weevils and flowering plants. Proc Natl Acad Sci U S A. 2009; 106:7083–8. [PubMed: 19365072]

22. Looney BP, Ryberg M, Hampe F, Sánchez-García M, Matheny PB. Into and out of the tropics: global diversification patterns in a hyperdiverse clade of ectomycorrhizal fungi. Mol Ecol. 2016; 25:630–647. [PubMed: 26642189]

23. Krah F-S, et al. Evolutionary dynamics of host specialization in wood-decay fungi. BMC Evol Biol. 2018; 18:119. [PubMed: 30075699]

24. Beaulieu JM, O'Meara BC. Extinction can be estimated from moderately sized molecular phylogenies. Evolution (N. Y). 2015; 69:1036–1043.

25. Rabosky DL. Challenges in the estimation of extinction from molecular phylogenies: A response to Beaulieu and O'Meara. Evolution (N. Y). 2016; 70:218–228.

26. Rabosky DL. Extinction rates should not be estimated from molecular phylogenies. Evolution (N. Y). 2010; 64:1816–1824.

27. May MR, Hohna S, Moore BR. A Bayesian approach for detecting the impact of mass-extinction events on molecular phylogenies when rates of lineage diversification may vary. Methods Ecol Evol. 2016; 7:947–959.

28. Tennant JP, Mannion PD, Upchurch P, Sutton MD, Price GD. Biotic and environmental dynamics through the Late Jurassic-Early Cretaceous transition: evidence for protracted faunal and ecological turnover. Biol Rev. 2017; 92:776–814. [PubMed: 26888552]

29. Casadevall A. Fungi and the Rise of Mammals. PLoS Pathog. 2012; 8:e1002808. [PubMed: 22916007]

30. Vajda V, McLoughlin S. Fungal Proliferation at the Cretaceous-Tertiary Boundary. Science (80-.). 2004; 303:1489–1489.

31. Mittelbach GG, et al. Evolution and the latitudinal diversity gradient: Speciation, extinction and biogeography. Ecology Letters. 2007; 10:315–331. [PubMed: 17355570]

32. Peay KG, Kennedy PG, Talbot JM. Dimensions of biodiversity in the Earth mycobiome. Nat Rev Microbiol. 2016; 14:434–447. [PubMed: 27296482]

33. Shi L-L, et al. Variation in forest soil fungal diversity along a latitudinal gradient. Fungal Divers. 2014; 64:305–315.

34. Tedersoo L, et al. Global diversity and geography of soil fungi. Science (80-.). 2014; 346:1256688–1256688.

35. Sánchez-Ramírez S, Etienne RS, Moncalvo JM. High speciation rate at temperate latitudes explains unusual diversity gradients in a clade of ectomycorrhizal fungi. Evolution (N. Y). 2015; 69:2196–2209.

36. Gavrilets S, Losos JB. Adaptive radiation: Contrasting theory with data. Science. 2009; 323:732–737. [PubMed: 19197052]

37. Givnish TJ. Adaptive radiation versus 'radiation' and 'explosive diversification': Why conceptual distinctions are fundamental to understanding evolution. New Phytol. 2015; 207:297–303. [PubMed: 26032979]

38. Maddison WP, Midford PE, Otto SP. Estimating a binary character's effect on speciation and extinction. Syst Biol. 2007; 56:701–710. [PubMed: 17849325]

39. Fitzjohn RG. Diversitree: Comparative phylogenetic analyses of diversification in R. Methods Ecol Evol. 2012; 3:1084–1092.

40. Berendse F, Scheffer M. The angiosperm radiation revisited, an ecological explanation for Darwin's 'abominable mystery'. Ecol Lett. 2009; 12:865–72. [PubMed: 19572916]

41. Niklas KJ, Tiffney BH, Knoll AH. Patterns in vascular land plant diversification. Nature. 1983; 303:614–616.

42. Berner RA. Phanerozoic atmospheric oxygen: New results using the GEOCARBSULF model. Am J Sci. 2009; 309:603–606.

43. Staden R. The Staden sequence analysis package. Mol Biotechnol. 1996; 5:233–241. [PubMed: 8837029]

44. CABI. Species Fungorum. Royal Botanic Gardens Kew. 2018

45. Knudsen H, V J. Funga Nordica. 2008

46. Loytynoja A, Goldman N. Phylogeny-Aware Gap Placement Prevents Errors in Sequence Alignment and Evolutionary Analysis. Science (80-.). 2008; 320:1632–1635.

47. Loytynoja A, Goldman N. From The Cover: An algorithm for progressive multiple alignment of sequences with insertions. Proc Natl Acad Sci. 2005; 102:10557–10562. [PubMed: 16000407]

48. Tóth A, et al. Iteratively Refined Guide Trees Help Improving Alignment and Phylogenetic Inference in the Mushroom Family Bolbitiaceae. PLoS One. 2013; 8

49. Gnerre S, et al. High-quality draft assemblies of mammalian genomes from massively parallel sequence data. Proc Natl Acad Sci. 2011; 108:1513–1518. [PubMed: 21187386]

50. Martin J, et al. Rnnotator: An automated de novo transcriptome assembly pipeline from stranded RNA-Seq reads. BMC Genomics. 2010; 11

51. Chin C-S, et al. Phased diploid genome assembly with single-molecule real-time sequencing. Nat Methods. 2016; 13:1050–1054. [PubMed: 27749838]

52. Lam K-K, LaButti K, Khalak A, Tse D. FinisherSC: a repeat-aware tool for upgrading *de novo* assembly using long reads. Bioinformatics. 2015; 31:3207–3209. [PubMed: 26040454]

53. Grigoriev IV, et al. MycoCosm portal: Gearing up for 1000 fungal genomes. Nucleic Acids Res. 2014; 42

54. Darling, A; Carey, L; Feng, W. The Design, Implementation, and Evaluation of mpiBLAST. 4th Int. Conf. Linux Clust. HPC Revolut. 2003 conjunction with Clust. Conf. Expo; 2003.

55. van Dongen, S. Graph Stimul by flow Clust. PhD thesis, University of Utrecht; 2000. Graph clustering by flow simulation.

56. Talavera G, Castresana J. Improvement of phylogenies after removing divergent and ambiguously aligned blocks from protein sequence alignments. Syst Biol. 2007; 56:564–577. [PubMed: 17654362]

57. Nagy LG, et al. Comparative genomics of early-diverging mushroom-forming fungi provides insights into the origins of lignocellulose decay capabilities. Mol Biol Evol. 2016; 33:959–970. [PubMed: 26659563]

58. Stamatakis A. RAxML version 8: A tool for phylogenetic analysis and post-analysis of large phylogenies. Bioinformatics. 2014; 30:1312–1313. [PubMed: 24451623]

59. Schliep KP. phangorn: phylogenetic analysis in R. Bioinformatics. 2011; 27:592–593. [PubMed: 21169378]

60. Lartillot N, Lepage T, Blanquart S. PhyloBayes 3: A Bayesian software package for phylogenetic reconstruction and molecular dating. Bioinformatics. 2009; 25:2286–2288. [PubMed: 19535536]

61. Åkerborg Ö, Sennblad B, Lagergren J. Birth-death prior on phylogeny and speed dating. BMC Evol Biol. 2008; 8

62. Smith SY, Currah RS, Stockey RA. Cretaceous and Eocene poroid hymenophores from Vancouver Island, British Columbia. Mycologia. 2004; 96:180–186. [PubMed: 21148842]

63. Hibbett DS, Grimaldi D, Donoghue MJ. Fossil mushrooms from Miocene and Cretaceous ambers and the evolution of homobasidiomycetes. Am J Bot. 1997; 84:981–991. [PubMed: 21708653]

64. Poinar G. Bird's nest fungi (Nidulariales: Nidulariaceae) in Baltic and Dominican amber. Fungal Biol. 2014; 118:325–329. [PubMed: 24607356]

65. Brown RW. A bracket fungus from the late Tertiary of southwestern Idaho. Journal of the Washington Academy of Sciences. 30:422–424.

66. Magallon-Puebla S, Cevallos-Ferriz SRS. A fossil earthstar (Geasteraceae; Gasteromycetes) from the Late Cenozoic of Puebla, Mexico. Am J Bot. 1993; 80:1162–1167.

67. Near TJ, Meylan PA, Shaffer HB. Assessing Concordance of Fossil Calibration Points in Molecular Clock Studies: An Example Using Turtles. Am Nat. 2005; 165:137–146. [PubMed: 15729646]

68. Charif, D, Lobry, JR. SeqinR 1.0-2: A Contributed Package to the R Project for Statistical Computing Devoted to Biological Sequences Retrieval and Analysis. Springer; Berlin, Heidelberg: 2007. 207–232.

69. Camacho C, et al. BLAST+: Architecture and applications. BMC Bioinformatics. 2009; 10:1–9. [PubMed: 19118496]

70. Sanderson MJ. Estimating absolute rates of molecular evolution and divergence times: a penalized likelihood approach. Mol Biol Evol. 2002; 19:101–109. [PubMed: 11752195]

71. Yang Z. PAML 4: Phylogenetic analysis by maximum likelihood. Mol Biol Evol. 2007; 24:1586–1591. [PubMed: 17483113]

72. Thorne JL, Kishino H, Painter IS. Estimating the rate of evolution of the rate of molecular evolution. Mol Biol Evol. 1998; 15:1647–1657. [PubMed: 9866200]

73. Bodensteiner P, Binder M, Moncalvo JM, Agerer R, S. Hibbett D. Phylogenetic relationships of cyphelloid homobasidiomycetes. Mol Phylogenet Evol. 2004; 33:501–515. [PubMed: 15336682]

74. Holt BG, et al. An Update of Wallace's Zoogeographic Regions of the World. Science (80-.). 2013; 339:74–78.

75. Core Team R. R: A language and environment for statistical computing. 2018.

76. Fitzjohn RG. Quantitative traits and diversification. Syst Biol. 2010; 59:619–633. [PubMed: 20884813]

77. Goldberg EE, Lancaster LT, Ree RH. Phylogenetic inference of reciprocal effects between geographic range evolution and diversification. Syst Biol. 2011; 60:451–465. [PubMed: 21551125]

78. Pagel M, Meade A. BayesTraits. 2007; 2

79. Pagel M. Inferring the historical patterns of biological evolution. Nature. 1999; 401:877–884. [PubMed: 10553904]

80. Xie W, Lewis PO, Fan Y, Kuo L, Chen MH. Improving marginal likelihood estimation for bayesian phylogenetic model selection. Syst Biol. 2011; 60:150–160. [PubMed: 21187451]

81. Revell LJ. phytools: An R package for phylogenetic comparative biology (and other things). Methods Ecol Evol. 2012; 3:217–223.

82. Huelsenbeck JP, Nielsen R, Bollback JP. Stochastic mapping of morphological characters. Syst Biol. 2003; 52:131–158. [PubMed: 12746144]

83. Wickham H. Ggplot2. Elegant Graphics for Data Analysis. 2009; doi: 10.1007/978-0-387-98141-3

84. Paradis E, Claude J, Strimmer K. APE: Analyses of phylogenetics and evolution in R language. Bioinformatics. 2004; 20:289–290. [PubMed: 14734327]

85. Fitzjohn RG, Maddison WP, Otto SP. Estimating trait-dependent speciation and extinction rates from incompletely resolved phylogenies. Syst Biol. 2009; 58:595–611. [PubMed: 20525612]

86. Rabosky DL, et al. BAMMtools: An R package for the analysis of evolutionary dynamics on phylogenetic trees. Methods Ecol Evol. 2014; 5:701–707.

87. Geweke J. Evaluating the accuracy of sampling-based approaches to the calculation of posterior moments. Bayesian Stat. 1992; 4:169–193.

88. Plummer M, Best N, Cowles K, Vines K. CODA: convergence diagnosis and output analysis for MCMC. R News. 2006; 6:7–11.

89. Nylander JAA, Wilgenbusch JC, Warren DL, Swofford DL. AWTY (are we there yet?): A system for graphical exploration of MCMC convergence in Bayesian phylogenetics. Bioinformatics. 2008; 24:581–583. [PubMed: 17766271]

90. Moore BR, Höhna S, May MR, Rannala B, Huelsenbeck JP. Critically evaluating the theory and performance of Bayesian analysis of macroevolutionary mixtures. Proc Natl Acad Sci. 2016; 113:9569–9574. [PubMed: 27512038]

91. Meyer ALS, Wiens JJ. Estimating diversification rates for higher taxa: BAMM can give problematic estimate of rates and rate shifts. Evolution (N. Y). 2017; :1–15. DOI: 10.1111/evo.13378

92. Magallon S, Sanderson MJ. Absolute diversification rates in angiosperms clades. Evolution (N. Y). 2001; 55:1762–1780.

93. Harmon LJ, Weir JT, Brock CD, Glor RE, Challenger W. GEIGER: Investigating evolutionary radiations. Bioinformatics. 2008; 24:129–131. [PubMed: 18006550]

94. Höhna S. The time-dependent reconstructed evolutionary process with a key-role for mass-extinction events. J Theor Biol. 2015; 380:321–331. [PubMed: 26073724]

95. Höhna S. Fast simulation of reconstructed phylogenies under global time-dependent birth-death processes. Bioinformatics. 2013; 29:1367–1374. [PubMed: 23543414]

96. Hohna, S; May, MR; Moore, BR. Phylogeny Simulation and Diversification Rate Analysis with TESS; 2015. 1–98. https://cran.r-project.org/web/packages/TESS/vignettes/Bayesian_Diversification_Rate_Analysis.pdf

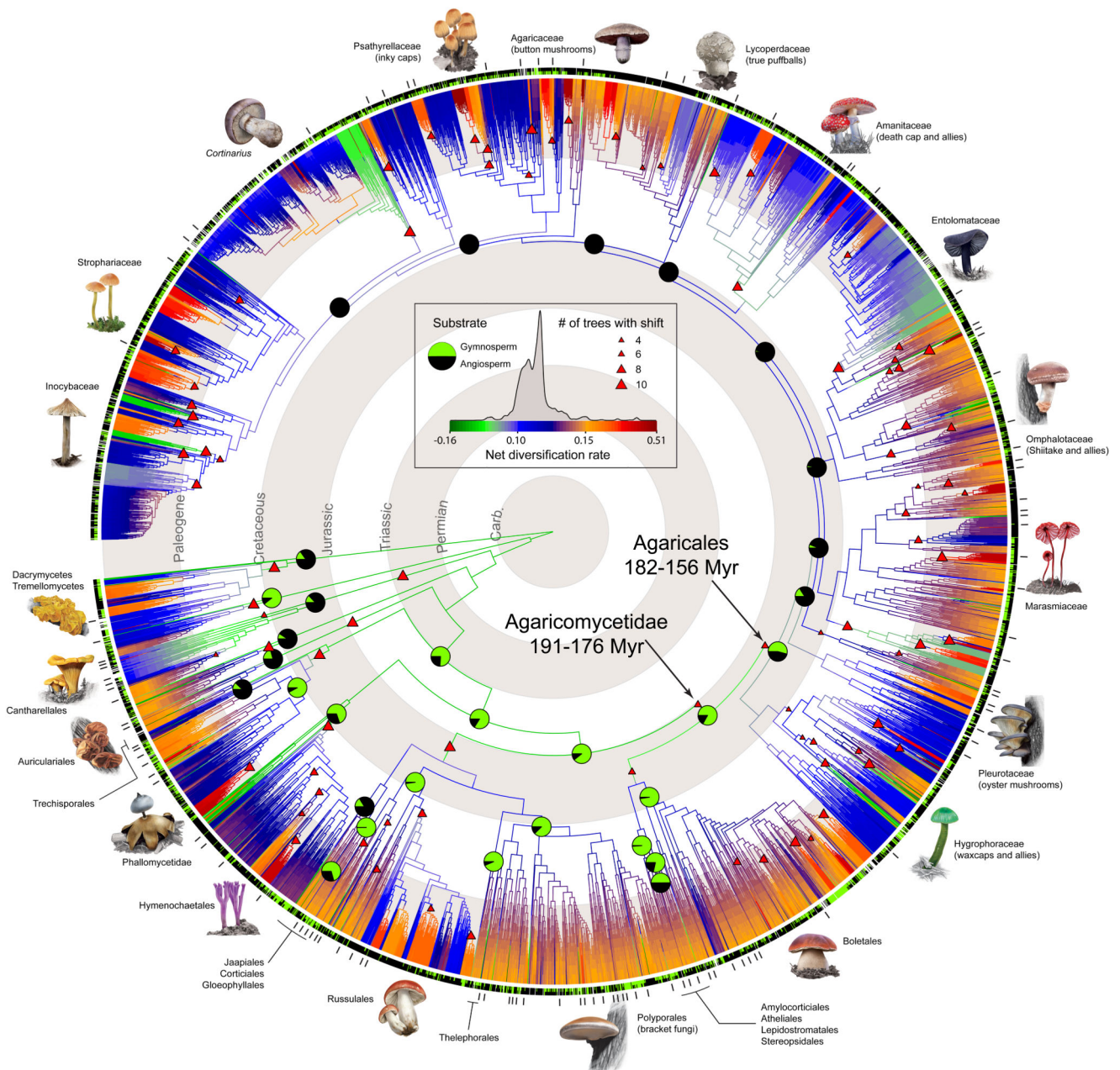97. Kass RE, Raftery AE. Bayes factors. J Am Stat Assoc. 1995; 90:773–795.

Figure 1.

Phylogenetic relationships and diversification across 5,284 mushroom-forming fungi. One of the 245 analyzed maximum likelihood trees was randomly chosen and visualized. Trees were inferred from nrLSU, *rpb2, ef1-a* sequences with a phylogenomic backbone constraint of deep nodes. Branches are colored by net diversification (speciation minus extinction) rate inferred in BAMM. Warmer colors denote a higher rate of diversification. Significant shifts in diversification rate are shown by triangles at nodes. Only shifts present on >50% of 10 analyzed trees, with a Bayesian posterior probability >0.5 and a posterior odds ratio >5 are shown. See Data 6 for detailed discussion of shifts. Reconstructed probabilities of ancestral plant hosts for order-level clades are shown as pie charts partitioned by the inferred ancestral

probability for gymnosperm (green) and angiosperm host (black). Pie charts are given for the most recent common ancestors of each order plus backbone nodes within the Agaricales – for small orders see Supplementary Data 3. Inner and outer bars around the tree denote extant substrate preference (black – angiosperm, green – gymnosperm, grey – generalist) and the placement of species used for inferring the 650-gene phylogenomic backbone phylogeny. Geological time scale is indicated with gray/white concentric rings.
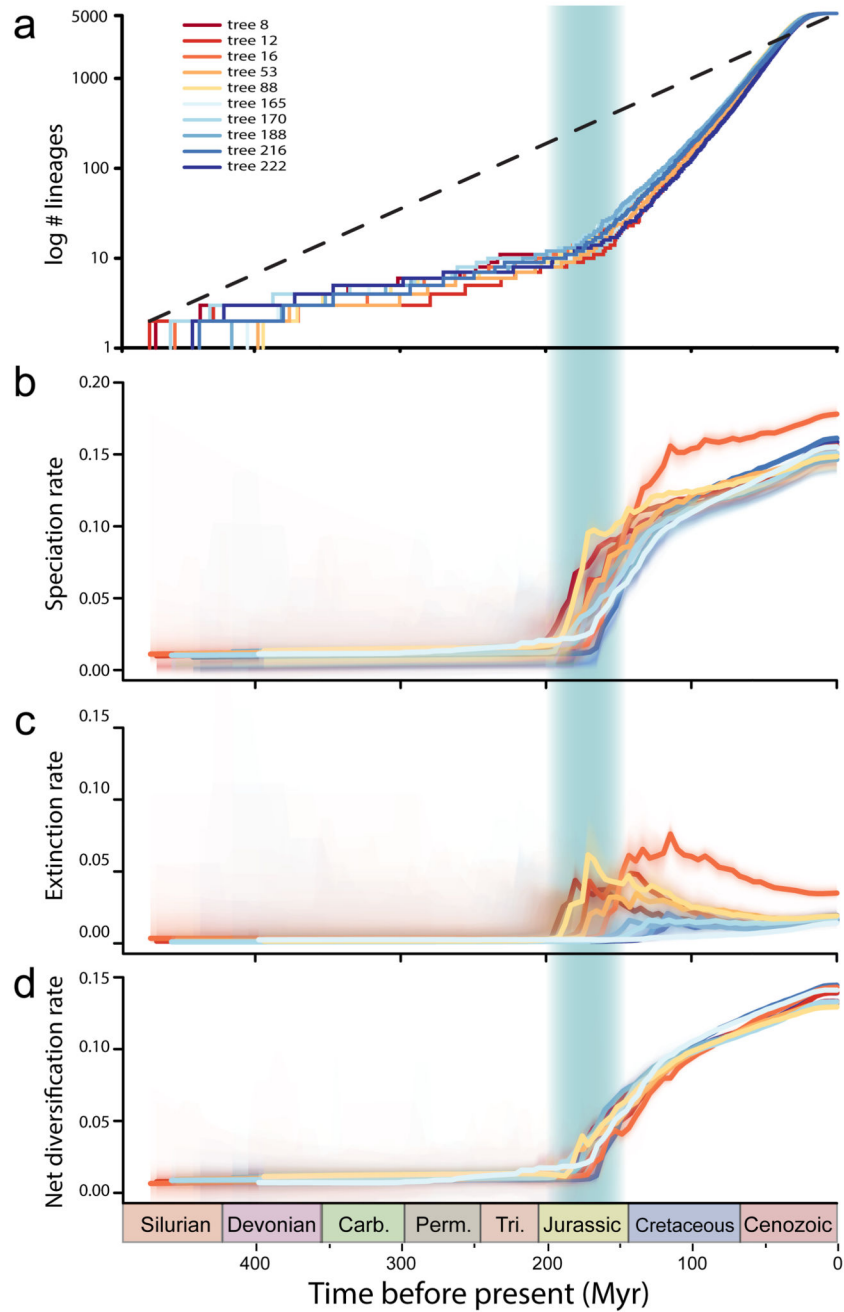
Figure 2.
Patterns of diversification of mushroom-forming fungi through time. (a) lineages through time plot, showing the log number of lineages through time, (b) speciation rate, (c) extinction rate and (d) net diversification rate through geologic time estimated using BAMM on ten chronograms comprising 5,284-species. 95% confidence intervals of rate estimates are shown by shaded areas. The Jurassic period is shaded in green.
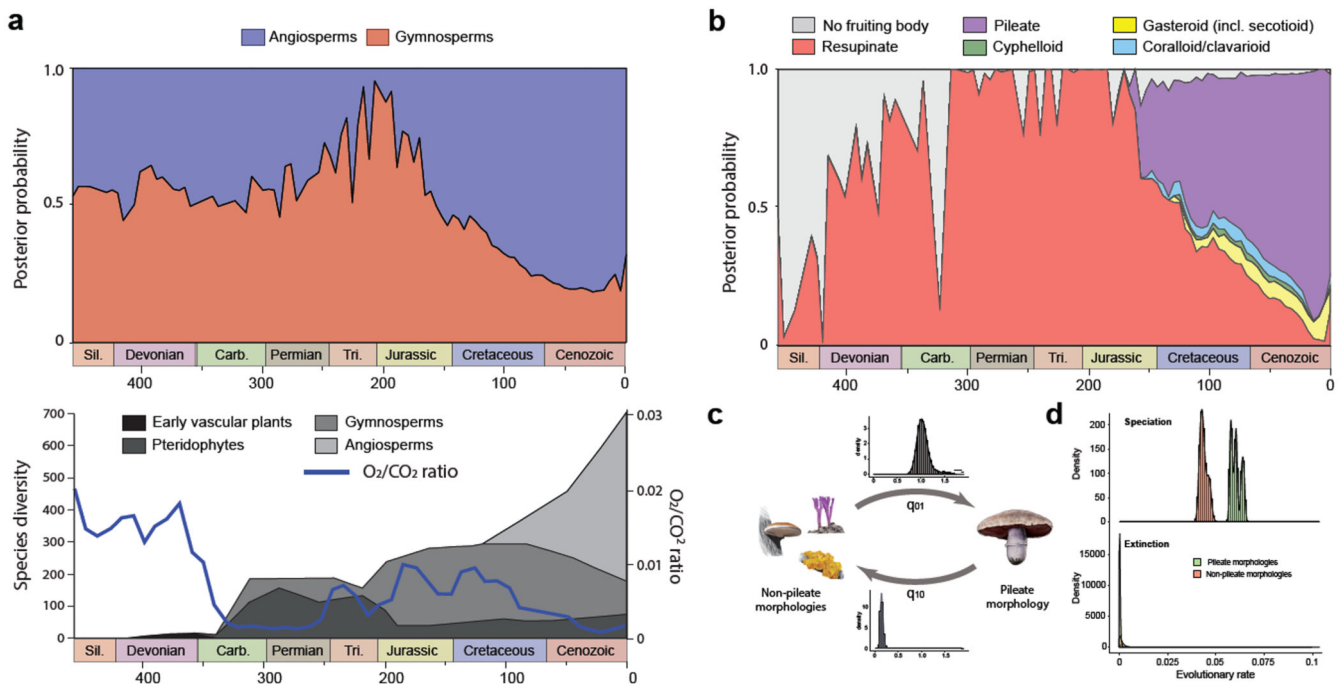
Figure 3.

The evolution of morphological and nutritional traits of mushrooms through time. (a) the evolution of substrate association through geologic time (top) and the evolution of vascular plant diversity and O_2/CO_2 levels (bottom, adapted from Niklas41 and Berner42. Plot created the as in Fig3/a. (b) the evolution of fruiting body types through time and the radiation of the agaricoid morphology since the Jurassic. Inferred ancestral probabilities of fruiting body types were summarized across the 10 phylogenies, by splitting the time scale of each tree into 100 bins and summing probabilities across the tree. For details of character coding and ancestral state reconstructions and detailed results, see Supplementary Note 5. (c) schematic model of the evolution of pileate-stipitate morphologies. The posterior distribution of transition rates from non-pileate (left) towards pileate-stipitate forms (right) and vice versa are shown above the arrows. Rates were estimated by MCMC in BayesTraits. (d) posterior distribution of trait-dependent speciation and extinction rates estimated under the binary state speciation and extinction model for non-pileate vs pileate-stipitate fruiting body morphologies.